Improved vertical-scanning interferometry

Akiko Harasaki, Joanna Schmit, and James C. Wyant

We describe a method that combines phase-shifting and coherence-peak-sensing techniques to permit measurements with the height resolution of phase-shifting interferometry without the interval-slope limitation of $\lambda/4$ per data sample of phase-shifting interferometry. A five-frame algorithm is used to determine both the best-focus frame position and the fractional phase from the best-focus frame of the correlogram acquired through vertical scanning. The two surface profiles retrieved from the phase and the modulation contrast of the correlograms are compared in the phase-unwrapping process to remove fringe-order ambiguity. © 2000 Optical Society of America

OCIS codes: 120.6650, 120.6660, 120.5050, 180.3170.

1. Introduction

Phase-shifting interferometry[1–5] (PSI) accompanied by large CCD arrays and powerful, low-cost computers can obtain measurements with a precision as high as $\lambda/1000$. However, PSI suffers from phase-ambiguity problems that limit the height difference between two adjacent data points to $\lambda/4$, where λ is the wavelength of the light used. One technique that has been successful in extending this height-difference limitation is multiple-wavelength interferometry.[6–9] Multiple-wavelength interferometry provides the precision of the wavelengths in use and the dynamic range of the equivalent wavelength, given by

$$\lambda_{eq} = \frac{\lambda_1 \lambda_2}{|\lambda_1 - \lambda_2|}. \quad (1)$$

Thus, by the selection of the two wavelengths it is possible to increase the dynamic range to hundreds and even to thousands of micrometers. This approach is an excellent method for measuring step heights[7]; however, it does not work especially well with rough surfaces.[10] On the other hand, a broad range of wavelengths and the coherence-peak-sensing approach[11–22] work quite well with rough surfaces but are less precise. Because of the large spectral bandwidth of the source, the coherence length is short, and high-contrast fringes are obtained only when the two path lengths of the interferometer are closely matched in length. The interference intensity distribution along the vertical-scanning direction, here called a correlogram, is attenuated by the coherence envelope with its peak (best-contrast fringes) at approximately the best-focus position.

There are many algorithms[16–22] for finding the coherence peak that lead to improved height resolution. To keep the time required for measuring and computing reasonable when measuring deep surfaces, it is necessary to sample the correlograms at or below twice the Nyquist frequency. However, these algorithms do not provide correct surface heights when the object being measured has a steplike discontinuity with a height less than the coherence length of the broadband light source.[23] A diffraction effect at the discontinuity causes the coherence envelope of the correlogram to skew and the peak to shift. This false information is referred to as bat wings because of its appearance in plotted measurements. The surface heights processed by well-established coherence-peak-sensing algorithms[14,15,17,19,22] appear to be higher (lower) when close to the top (bottom) of the step discontinuity, as shown in Fig. 1. It can be shown that diffraction effects modify the coherence envelope more than the phase[23] of the correlogram. Thus phase measurement is preferred when steplike discontinuities cause bat wings.

It is very natural to arrive at the idea that combining PSI with coherence-peak sensing might provide the advantages of both methods, i.e., high precision and a large dynamic range, and, in addition, overcome the bat-wing effect. Larkin[18] and Sandoz *et al.*[24] proposed white-light phase-shifting interferom-

The authors are with the Optical Sciences Center, University of Arizona, Tucson, Arizona 85721. J. Schmit is also with Veeco Process Metrology, 2650 East Elvira Road, Tucson, Arizona 85706. A. Harasaki's e-mail address is harasaki@u.arizona.edu.

Received 10 September 1999; revised manuscript received 4 February 2000.

0003-6935/00/132107-09$15.00/0

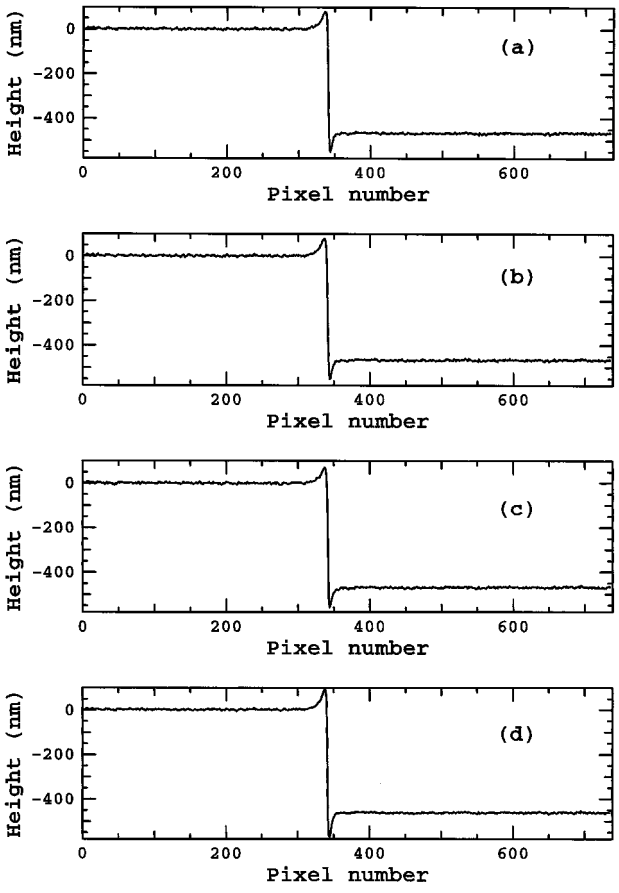

Fig. 1. Surface profiles of the 460-nm height standard (VLSI, SHS 4600 Å) processed by (a) the centroid algorithm,[19] (b) from the centroid of the recovered modulation contrast by the Fourier transform algorithm,[14] (c) from the centroid of the recovered modulation contrast by the Hilbert transform algorithm,[15] (d) from the phase slope in the Fourier domain.[17,22]

etry[25] (WLPSI) to achieve unambiguous and nanometric-resolution measurement of objects. Their idea is that one can find the best-focus frame position by locating the largest modulation-contrast position of the coherence envelope of correlograms and at the same time measuring the fractional phase from the best-focus frame position. Sandoz *et al.*[24] showed great height-resolution improvement when measuring a tilted smooth surface and a deep silicon sample. However, to our knowledge, no experimental results have been reported that show that bat wings can be removed.

This paper presents a simple WLPSI algorithm that yields a large dynamic range and high-precision measurement and removes the bat-wing effect. It also removes the phase ambiguities that monochromatic interferometry and WLPSI are prone to.

2. Phase Measurement from the Coherence-Peak Position

Two of the earliest-documented automated methods for determining three-dimensional information from white-light correlograms are reported in a patent by Balsubramanian[11] and a paper by Davidson *et al.*[12] Today, there are at least 10 different metrology companies competing in this growing market. Although a considerable number of papers describing algorithms[13–22] that retrieve three-dimensional information from white-light correlograms exist, not all have been published in detail.

The main concern in correlogram analysis is how to find the coherence peak from the discrete intensity data points without limiting the height resolution to the scanning-step distance.[16–22] For the purpose of further improving the height resolution the phase information, called the fractional phase, in a white-light correlogram is extracted from the best focus, i.e., the highest-contrast axial-scanning position, by use of the PSI algorithms proposed in WLPSI techniques. The phase information is expected to be more sensitive to height variations[18,24–26] than are any of the coherence-peak-sensing techniques. The measured fractional phase from the best-focus frame[26,27] may result in 2π phase ambiguities and has to be unwrapped to retrieve height information, which is an essential step in WLPSI methods. Sandoz *et al.*[24] introduced a fringe-order function to remove the 2π ambiguities that shows well-separated values for different fringe orders when the correlogram has such low noise that the assumption of local linearity of the coherence envelope is valid.

In this paper a more intuitive way to correct 2π ambiguities is proposed. Two profiles are obtained, one from the coherence-peak-sensing technique and the other from phase measurement at the best-focus frame position. The two profiles are compared, and the phase ambiguities are removed, as described in Section 3. It is necessary to obtain a good profile from the coherence-peak-sensing technique to ensure that the unwrapping process works.

There are two ways to find the coherence-peak position between frames from the recovered discrete modulation-contrast data sets. One is a least-squares fitting method[16,18] that assumes a function form for the coherence envelope from the source distribution. The other is calculation of the centroid[14,15,19] of the correlogram. These two methods yield identical results for ideal noise-free correlograms. However, Larkin[18] showed that the centroid is more susceptible to noise. We show in Fig. 2(b) an example whose correlogram centroid is not a good estimator for the best-focus position. The centroid of the coherence-envelope function may shift away from the envelope peak at positions on or close to a discontinuity.[23] If the centroid shifts away from the coherence-envelope peak the obtained fractional phase may contain false information. As a result, the phase measurement should be taken from the actual coherence-peak position rather than from the centroid position.

3. Phase-Unwrapping Algorithm

To measure the fractional phase from the best-focus frame position, we first have to find the frame position with the maximum modulation contrast of the correlogram. The modulation contrast M at each

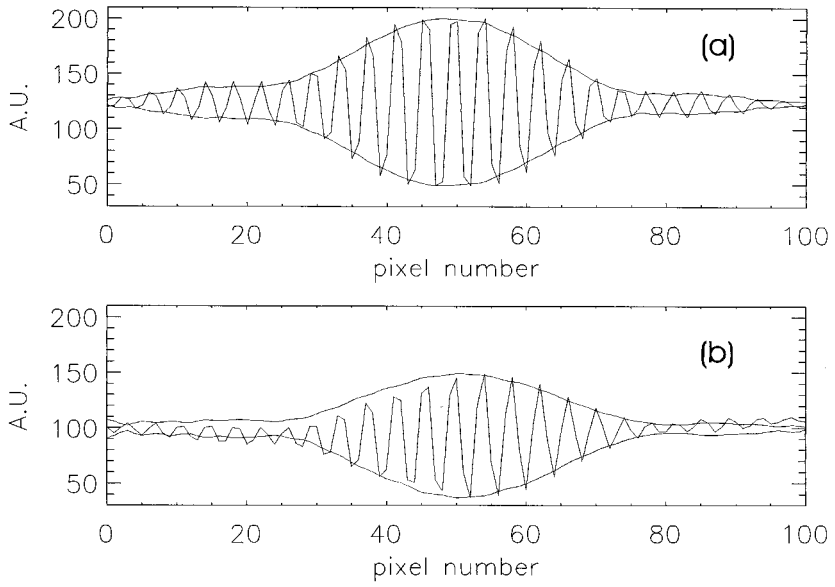

Fig. 2. Typical correlograms and their coherence envelopes obtained by use of the Mirau interference microscope: (a) Positioned far from the step edge. The peak position is 48.77, and the centroid position is 48.75. (b) Positioned on or close to the step edge. The peak position is 50.80, and the centroid position is 50.91.

pixel is calculated in accord with expression (2) at each step of scanning[18,28]:

$$M^2 \propto (I_2 - I_4)^2 - (I_1 - I_3)(I_3 - I_5). \tag{2}$$

The phase step α between frames is adjusted to 90° (a scanning step of $\Delta = \bar{\lambda}/8$, where $\bar{\lambda}$ is the mean wavelength) or to 270° (a scanning step of $\Delta = 3\bar{\lambda}/8$). I_1 through I_5 are five consecutive frames of intensity data measured for each pixel, as shown in Fig. 3.

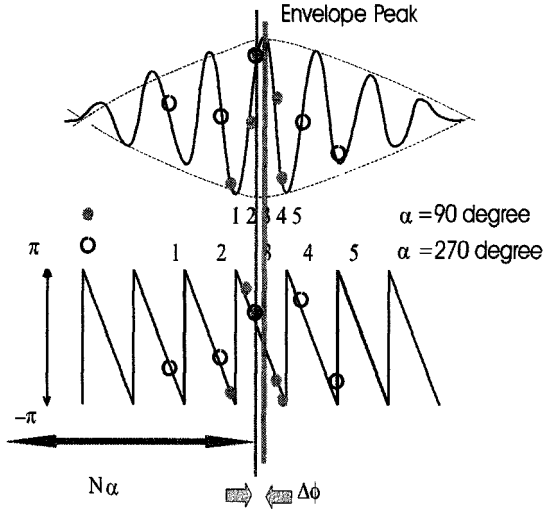

Fig. 3. Correlogram and its retrieved phase information obtained while the optical path difference is scanned. The filled circles indicate five consecutive intensity data points separated by a 90° phase shift (the scanning step is $\Delta = \bar{\lambda}/8$); the open circles indicate five consecutive intensity data points separated by a 270° phase shift (the scanning step is $\Delta = 3\bar{\lambda}/8$). The term $\Delta\phi$ is the relative phase from the best-focus position, and $N\alpha$ is the absolute best-focus position.

When the modulation is at its maximum the best-focus scanning-frame position (step number) is determined. Then the phase difference $\Delta\phi$ between the zero optical path difference and the best-focus scanning position is evaluated by use of a five-frame algorithm:

$$\tan(\Delta\phi) = 2 \sin \alpha \frac{I_2 - I_4}{2I_3 - I_5 - I_1}, \tag{3}$$

$$\sin^2 \alpha = \frac{4(I_2 - I_4)^2 - (I_1 - I_5)^2}{4(I_2 - I_4)^2}. \tag{4}$$

The surface height is then expressed as

$$z_{\text{phase}}(x, y) = \Delta(\text{step number}) + \frac{f}{2}\left(\frac{\Delta\phi\bar{\lambda}}{2\pi}\right), \tag{5}$$

where f is the so-called numerical-aperture (NA) factor. The NA of an interferometric microscope objective can affect the fringe spacing and thus the surface heights measured with that objective.[29,30] The NA factor in Eq. (5) takes care of this effect.

Sandoz *et al.*[24] point out that the phase ambiguity in Eq. (3) can be avoided if the central intensity I_3 is recorded within the zero-order fringe. However, it is difficult to ensure this condition, especially for the 270° phase step between frames. Thus Eq. (5) should be rewritten as

$$z_{\text{phase}}(x, y) = \Delta(\text{step number}) + \frac{f}{2}\left[\frac{(\Delta\phi + 2k\pi)\bar{\lambda}}{2\pi}\right], \tag{6}$$

where k is the fringe order that has to be determined in the unwrapping process.

In this paper, we propose the removal of the phase

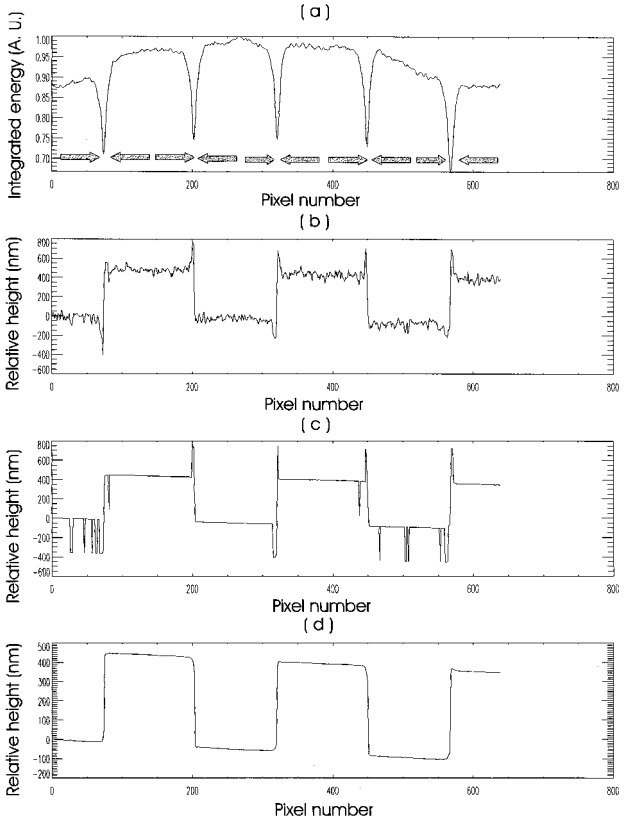

Fig. 4. Processed surface profile of a 460-nm height standard (VLSI, SHS 4600 Å): (a) The energy distribution along the pixel positions. (b) The surface profile obtained by use of Eq. (7). (c) The surface profile obtained by use of Eq. (5). (d) The resultant unwrapped surface profile.

ambiguity from $z_{\text{phase}}(x, y)$ by introducing a surface profile, $z_{\text{envelope}}(x, y)$, that is obtained from a coherence-peak-sensing technique as a reference. One can calculate the reference surface profile by first finding the best-focus frame. Then the peak location of the coherence envelope is calculated from the best-focus frame by use of least-squares fitting of the modulation contrast.[18] Therefore our reference profile can be expressed as

$$z_{\text{envelope}}(x, y) = \Delta(\text{step number}) + \Delta z, \tag{7}$$

where

$$\Delta z = 0.4\Delta \frac{L_1 + 3L_2 - 3L_4 - L_5}{L_1 - 2L_3 + L_5} \tag{8}$$

and L_n represents the logarithm of the modulation-contrast value M_n. The small correction Δz is important to ensure that the phase-unwrapping process works. Simply comparing the surface profile $z_{\text{phase}}(x, y)$ with the other surface profile $z_{\text{envelope}}(x, y)$ can lead to the removal of the 2π ambiguity [$(f/2)\bar{\lambda}$ in height] from $z_{\text{phase}}(x, y)$, and the resultant height resolution is as good as that obtained through regular PSI.[1–5]

The 2π phase ambiguities can be removed in three steps. In the first step the phase-unwrapping process should start from a reliable position, for example, by use of the modulation contrast of correlograms as an indicator of a smooth surface. However, we found that integrating the energy through the vertical scan shown in Fig. 4(a) could be a better indicator of a surface with discontinuities to avoid suspicious positions. The energy reduction is clear at positions close to the edges in the height standard [VLSI, SHS (step-height standard) 4600 Å], which has a 460.6-nm step and same-height wells on the surface. For this particular sample the unwrapping is done from the relatively high-energy positions to the energy minimums, as illustrated by the arrows in Fig. 4(a). Figures 4(b) and 4(c) show the surface profile calculated from Eq. (7) and Eq. (5), respectively. Bat wings are significant in the coherence-peak-sensing technique, as expected, because the coherence length of the light source[31] is larger than the step height. We can clearly see at this point that the integrated energy is a very good indicator of the possibility of the existence of bat wings.[23]

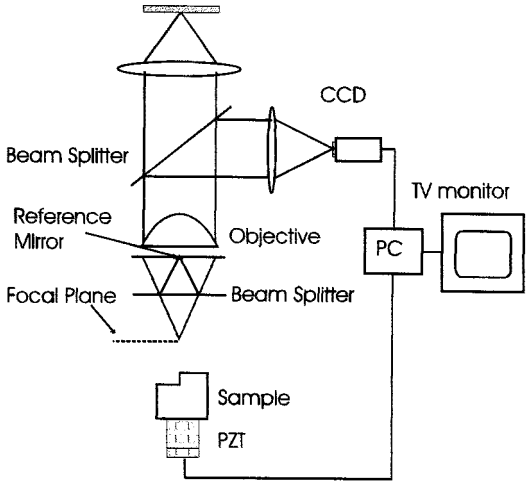

Fig. 5. Experimental setup with the Mirau interference microscope (Veeco, Model WYKO NT-2000). A broadband light source with a center wavelength of 600 nm and a bandwidth of 80 nm is used. PZT, piezoelectric transducer.

In the second step, $z_{\text{phase}}(i)$ and $z_{\text{envelope}}(i)$ are compared at the lateral position i to see if the height difference between them is less than than $(f/4)\bar{\lambda}$, i.e.,

$$|z_{\text{phase}}(i) - z_{\text{envelope}}(i) + \text{offset}| \leq \frac{f}{4}\bar{\lambda}. \tag{9}$$

If condition (9) is not satisfied $(f/2)\bar{\lambda}$ needs to be added to or subtracted from the surface height obtained from Eq. (5) until the condition is met. The offset can be estimated if the average is taken of the difference of the two surface profiles, i.e., offset $\simeq 1/N \sum_{i=1}^{N} [z_{\text{envelope}}(i) - z_{\text{phase}}(i)]$. The offset takes care of the constant phase shift on reflection, although we do not need to know it or to measure it. The process described by relation (9) is effective for the continuous portion of the surface but cannot remove the 2π

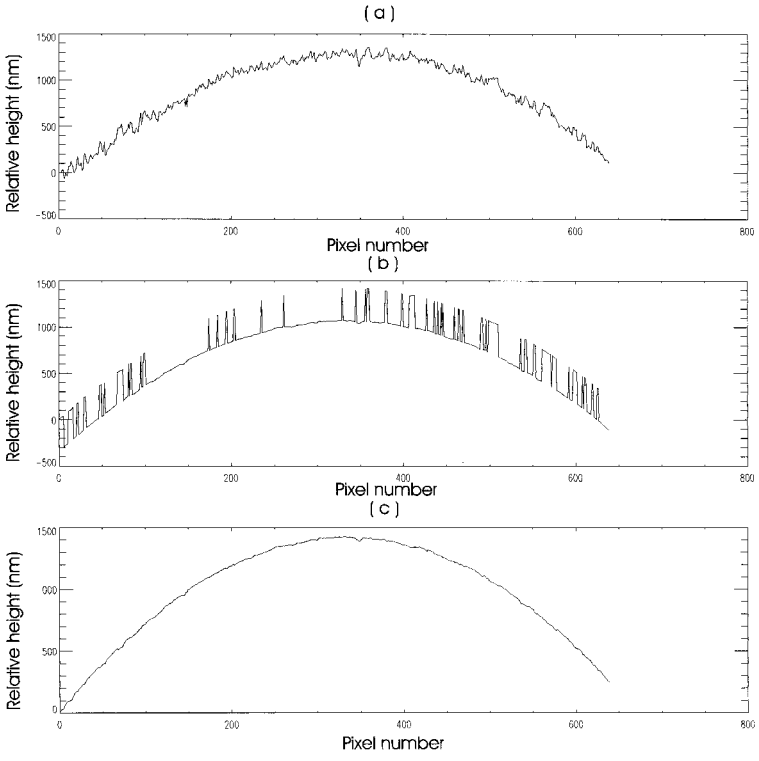

Fig. 6. Surface profile of a ball bearing obtained by use of 90° white-light phase shifting: (a) Determined with the coherence-peak-sensing technique with Eq. (7). (b) Determined with Eq. (5). (c) Final result after 2π phase correction.

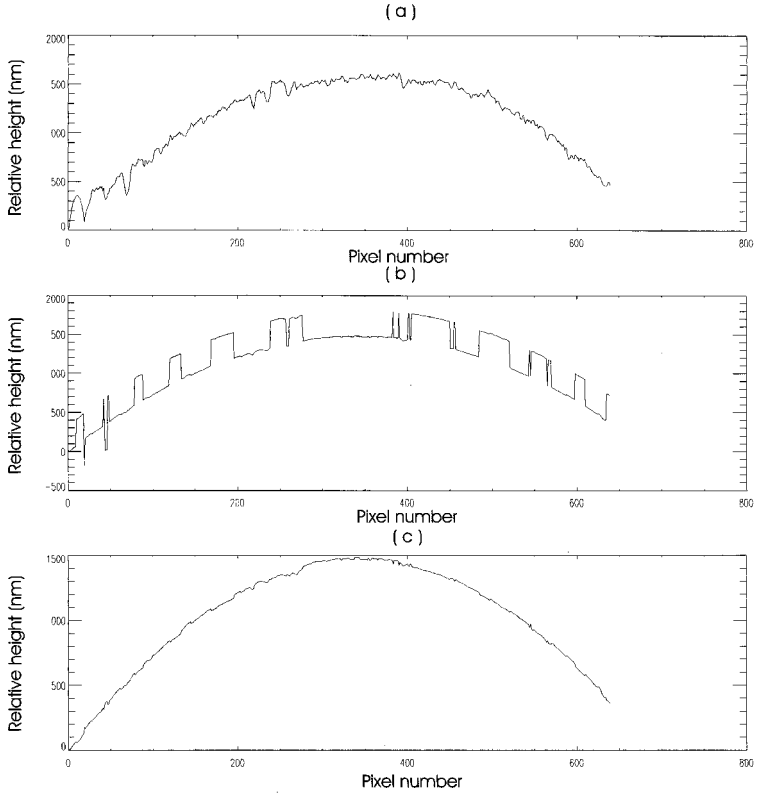

Fig. 7. Surface profile of a ball bearing obtained by use of 270° white-light phase shifting: (a) Determined with the coherence-peak-sensing technique with Eq. (7). (b) Determined with Eq. (5). (c) Final result after 2π phase correction.

Table 1. Surface-Roughness Parameters of a Ball Bearing for Two Algorithms

Algorithm	90° Phase Shifting (nm)		270° Phase Shifting (nm)		Rms Deviation (nm)
	R_a	R_q	R_a	R_q	
Coherence-peak sensing[a]	36	45	41	56	68
Phase shifting[b]	9	11	14	16	14

[a]Based on Eq. (7) in Ref. 18.
[b]Based on Eq. (5) after unwrapping.

jumps at positions close to the edges because of the bat-wing effect.

The third step in the unwrapping procedure is taken to remove the bat-wing effect. For the positions at which the height difference between two adjacent points in z_{envelope} is smaller than $(f/4)\bar{\lambda}$ and the difference in z_{phase} is larger than $(f/4)\bar{\lambda}$, such that

$$|z_{\text{envelope}}(i) - z_{\text{envelope}}(i-1)| < \frac{f}{4}\bar{\lambda},$$

$$|z_{\text{phase}}(i) - z_{\text{phase}}(i-1)| > \frac{f}{4}\bar{\lambda}, \tag{10}$$

$n(f/2)\bar{\lambda}$ is added to or subtracted from z_{phase} to satisfy the conditions

$$|z_{\text{envelope}}(i) - z_{\text{envelope}}(i-1)| < \frac{f}{4}\bar{\lambda},$$

$$|z_{\text{phase}}(i) - z_{\text{phase}}(i-1)| < \frac{f}{4}\bar{\lambda}. \tag{11}$$

Figure 4(d) shows the surface profile after the full correction process. We can see that both the 2π jumps and the bat wings are completely removed. Consequently, a great improvement in surface resolution is achieved. It is questionable whether the correction process described by expressions (10) and (11) works when the bat-wing height changes by more than $f\bar{\lambda}/4$ between data points. The bat wings usually have a lateral extension over several pixels, and the maximum height is less than 200 nm (Ref. 23) when measured with a white-light source that has a mean wavelength near 600 nm. Therefore we can assume that the bat wings introduce an error to the height difference between two adjacent data points of less than $f\bar{\lambda}/4$ for most cases.

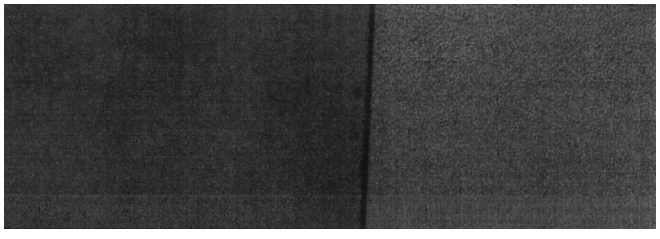

Fig. 8. Camera image of the step-height standard (VLSI, SHS 4600 Å). Note the structure close to the step edge.

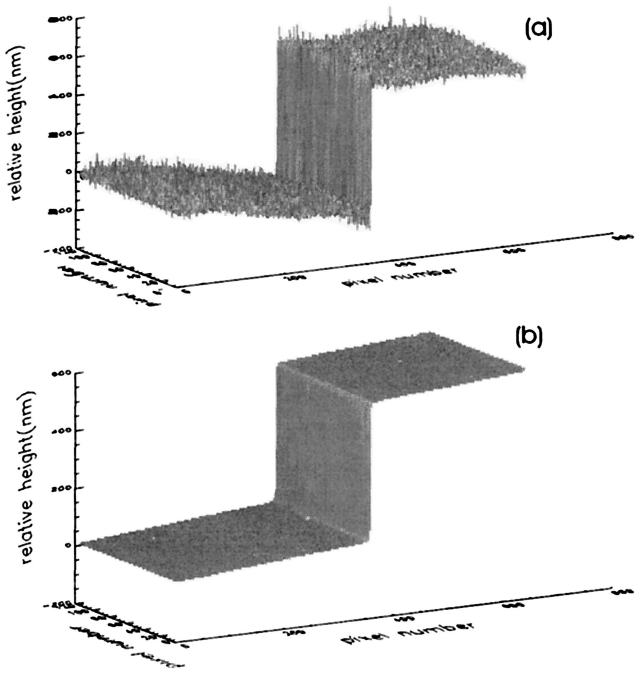

Fig. 9. Processed surface profile of the step-height standard (VLSI, SHS 4600 Å). The measurement was performed with an 80-nm bandpass filter at the center wavelength of 600 nm: (a) The profile obtained by use of the regular coherence-peak-sensing algorithm.[18] (b) The profile obtained by use of the proposed white-light phase-shifting algorithm.

At this point it is prudent to discuss situations in which the proposed method works and those in which it does not. As was mentioned above, this method requires a good surface profile from the coherence-peak-sensing measurement, which should not be randomly off by more than $f\bar{\lambda}/4$. In other words, if the surface profile calculated by use of Eq. (7) is not meaningful the proposed algorithm probably will not work well. One situation in which the algorithm does not work well is with periodic structures like gratings that diffract the illuminating light away from the system so that the signal-to-noise ratio is so low that it is difficult to produce the correct surface profile from the modulation contrast of the correlograms.

4. Experimental Results

Experiments were carried out with a Mirau interference microscope (Veeco, Model WYKO NT-2000), as illustrated in Fig. 5. A Nikon 50× magnification objective (NA = 0.55) was used because bat-wing effects are significant for large NA's.[23] Correlograms were detected by a CCD video camera. A piezoelectric transducer (Queensgate Instruments, Model NPS-Z-15B, stage position) was used instead of the high-precision motor in the commercial version of the Model WYKO NT-2000 for vertical scanning. The piezoelectric transducer was used because equally spaced scanning steps between frames are

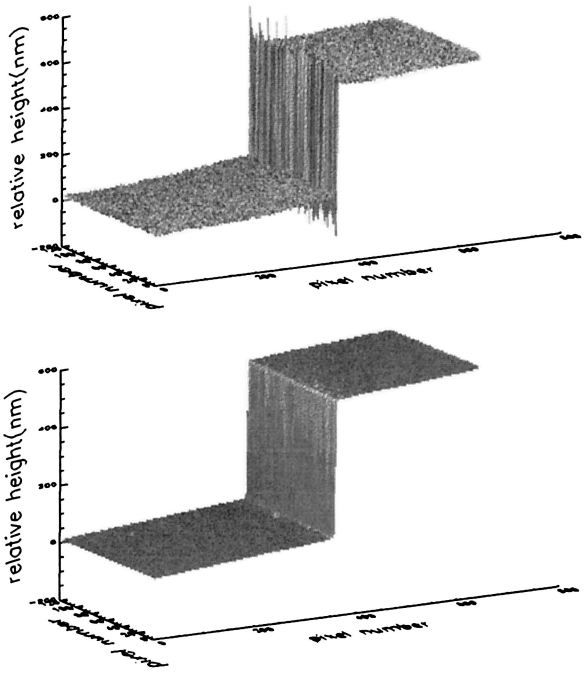

Fig. 10. Processed surface profile of the step-height standard (VLSI, SHS 4600 Å). The measurement was performed with an unfiltered tungsten light source: (a) The profile obtained by use of the regular coherence-peak-sensing algorithm.[18] (b) The profile obtained by use of the proposed white-light phase-shifting algorithm.

required to minimize phase-shifting errors.[1,2] A high-precision motor can be used for scanning through samples that have surface structures larger than millimeters as long as the errors caused by the motor have been measured and can be removed by signal-processing techniques.[3,4,18,28,32] The broadband light source was either an unfiltered tungsten bulb or a filtered source with a center wavelength at 600 nm and an 80-nm bandwidth. The former gives better resolution in the coherence-peak-sensing technique,[5,11–22] and the latter is preferred for PSI[1–5] with high-magnification objectives.

Figures 6 and 7 present measured surface profiles of a ball bearing, which cannot be measured by the regular phase-shifting technique with high-magnification objectives because the objective's depth of focus is less than the depth of the sample. Figures 6(a) and 7(a) show the results obtained by use of the coherence-peak-sensing technique according to Eq. (6), Figs. 6(b) and 7(b) show the raw output obtained by use of Eq. (5), and Figs. 6(c) and 7(c) show the final result after 2π phase correction with the algorithm proposed in Section 3.

Table 1 summarizes the roughness average R_a and the rms roughness R_q, which are defined as

$$R_a = \frac{1}{N}\sum_{i=1}^{N} |z(i) - z_{\text{fit}}(i)|, \tag{12}$$

$$R_q = \left\{\frac{1}{N}\sum_{i=1}^{N} [z(i) - z_{\text{fit}}(i)]^2\right\}^{1/2}, \tag{13}$$

where z_{fit} is found by the fitting of the sag equation to the mean averages of the surface heights of Figs. 6(a), 6(c), 7(a), and 7(c). The rms deviations for different techniques between the 90° and the 270° phase-shift results are estimated and listed in Table 1 and can be an indicator of the repeatability of an algorithm. The numbers here do not give the absolute accuracy for the method proposed. They indicate that indeed the height resolution can be improved by use of the proposed algorithm as compared with the resolution of the regular coherence-peak-sensing technique.

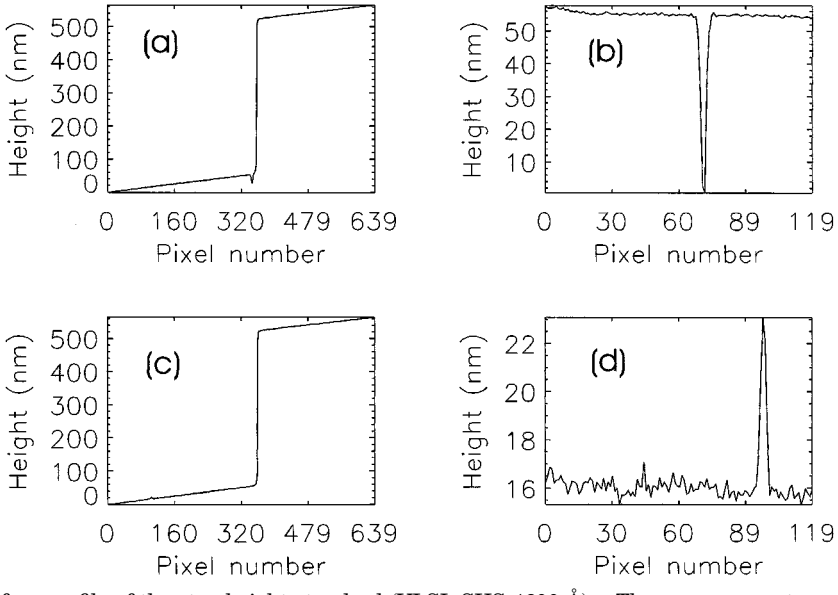

Fig. 11. Processed surface profile of the step-height standard (VLSI, SHS 4600 Å). The measurement was performed with an 80-nm bandpass filter at the center wavelength of 600 nm: (a) The x profile and (b) the y profile of the hole close to the step edge at position (346, 69). (c) The x profile and (d) the y profile of a small bump at position (104, 96) far toward the left-hand side of Fig. 8.

As was stated in Section 3 the proposed method is capable of removing the bat wings and revealing the surface structure on or close to the edges. A step-height standard (VLSI, SHS 4600 Å) measurement was conducted to demonstrate this effect. The camera images of the step are shown in Fig. 8. Figures 9 and 10 show the processed profiles obtained by use of the method proposed in this paper for filtered and unfiltered tungsten sources, respectively. The surface profiles from the regular coherence-peak-sensing technique are also shown in Figs. 9 and 10 for comparison. The height-resolution improvement is obvious, and the bat wings are completely removed. In Fig. 8 on the left-hand side (lower side of the step) there are two defects on the surface that have the appearance of stains. With the new method the two defects were characterized as a hole and a bump; such shape determination not possible with either the coherence-peak-sensing technique or the phase-shifting method by itself.

A detailed analysis is shown in Fig. 11 that was obtained by use of Veeco's software WYKO Vision32. The hole close to the step was found to measure 55 nm, and the bump far to the left-hand side was found to measure 7 nm. The results powerfully prove the advantages of the proposed WLPSI technique: high resolution and a large dynamic range.

Each month several papers are published on new algorithms for surface metrology, and the most important claim in many of these papers is how rapidly the algorithm can acquire and process surface information. From Section 3 it is clear that the computation time required for the WLPSI method proposed in this paper is the sum of the time for regular coherence-peak-sensing and phase-shifting calculations. Efforts in surface metrology over the past 30 years have yielded fast algorithms for calculating surface profiles by both the coherence-peak-sensing and the phase-shifting techniques, so the combined method proposed here is guaranteed to be a fast algorithm for practical requirements.

5. Conclusions

We have shown the advantages of using a white-light phase-shifting technique that possesses the accuracy of regular PSI without the $\lambda/4$ dynamic-range limitation. A simple phase-unwrapping algorithm has been proposed and applied to a 460-nm square well, a ball bearing, and a 460-nm step-height surface. The algorithm can remove the bat-wing effect and reveal surface structures that are close to the step edge.

The authors thank Veeco Corporation for providing the Mirau interference microscope (Model WYKO NT-2000). We also wish to thank Bob Knowlden of Veeco Corporation for helpful suggestions and discussions.

References and Notes

1. K. Creath, "Phase-measurement interferometry techniques," in *Progress in Optics XXVI*, E. Wolf, ed. (Elsevier, Amsterdam, The Netherlands, 1988), pp. 349–393.
2. J. E. Greivenkamp and J. H. Bruning, "Phase shifting interferometers," in *Optical Shop Testing*, D. Malacara, ed. (Wiley, New York, 1992), pp. 501–598.
3. J. Schmit and K. Creath, "Extended averaging technique for derivation of error-compensating algorithms in phase-shifting interferometry," Appl. Opt. **34,** 3610–3619 (1995).
4. P. de Groot, "Derivation algorithms for phase-shifting interferometry using the concept of a data-sampling window," Appl. Opt. **34,** 4723–4730 (1995).
5. J. C. Wyant and J. Schmit, "Computerized interferometric measurement of surface microstructure," in *Optical Inspection and Micromeasurements*, C. Gorecki, ed., Proc. SPIE **2782,** 26–37 (1996).
6. Y.-Y. Cheng and J. C. Wyant, "Two-wavelength phase shifting interferometry," Appl. Opt. **23,** 4539–4543 (1984).
7. K. Creath, "Step height measurement using two-wavelength phase-shifting interferometry," Appl. Opt. **26,** 2810–2816 (1987).
8. J. C. Wyant and K. Creath, "Two-wavelength phase-shifting interferometer and method," U.S. patent 4,832,489 (filed 19 March 1986; issued 23 May 1989).
9. P. J. de Groot, "Extending the unambiguous range of two-color interferometers," Appl. Opt. **33,** 5948–5953 (1994).
10. Rough surfaces have local steep slopes that result in narrow fringe spacings, so the condition of two detectors per fringe is easily violated. Compared with the step height, which consists of smooth surfaces and step discontinuities, the surface profile obtained by use of the two-wavelength PSI technique is less accurate.
11. N. Balsubramanian, "Optical system for surface topography measurement," U.S. patent 4,340,306 (filed 4 February 1980; issued 20 July 1982).
12. M. Davidson, K. Kaufman, I. Mazor, and F. Cohen, "An application of an interference microscope to integrated circuit inspection and metrology," in *Integrated Circuit Microscopy: Inspection and Process Control*, K. M. Monahan, ed., Proc. SPIE **775,** 233–247 (1987).
13. B. S. Lee and T. C. Strand, "Profilometry with a coherence scanning microscope," Appl. Opt. **29,** 3784–3788 (1990).
14. G. S. Kino and S. S. C. Chim, "Mirau correlation microscope," Appl. Opt. **29,** 3775–3783 (1990).
15. S. S. C. Chim and G. S. Kino, "Three-dimensional image realization in interference microscopy," Appl. Opt. **31,** 2550–2553 (1992).
16. P. J. Caber, "Interferometric profiler for rough surfaces," Appl. Opt. **32,** 3438–3441 (1993).
17. L. Deck and P. de Groot, "High-speed noncontact profiler based on scanning white-light interferometry," Appl. Opt. **33,** 7334–7338 (1994).
18. K. G. Larkin, "Effective nonlinear algorithm for envelope detection in white light interferometry," J. Opt. Soc. Am. A **13,** 832–843 (1996).
19. C. Ai and E. L. Novak, "Centroid approach for estimating modulation peak in broad-bandwidth interferometry," U.S. patent 5,633,715 (filed 19 May 1996; issued 27 May 1997).
20. P. Sandoz, "Wavelet transform as a processing tool in white-light interferometry," Opt. Lett. **22,** 1065–1067 (1997).
21. R. J. Recknagel and G. Notni, "Analysis of white light interferograms using wavelet methods," Opt. Commun. **148,** 122–128 (1998).
22. M. Hart, D. G. Vass, and M. L. Begbie, "Fast surface profiling by spectral analysis of white-light interferograms with Fourier transform spectroscopy," Appl. Opt. **37,** 1764–1769 (1998).
23. A. Harasaki and J. C. Wyant, "Fringe modulation skewing effect in white light vertical scanning interferometry," Appl. Opt. **39,** 2101–2106 (2000).
24. P. Sandoz, R. Devillers, and A. Plata, "Unambiguous profilometry by fringe-order identification in white-light phase-shifting interferometry," J. Mod. Opt. **44,** 519–534 (1997).

25. D. K. Cohen, P. J. Caber, and C. P. Brophy, "Rough surface profiler and method," U.S. patent 5,133,601 (filed 12 June 1991; issued 28 July 1992).
26. P. Hariharan and M. Roy, "White-light phase-stepping interferometry: measurement of the fractional interference order," J. Mod. Opt. **42,** 2357–2360 (1995).
27. Please refer to Fig. 3. The interferogram is taken every 90° (270°), which corresponds to a distance of $\bar{\lambda}/4$ ($3\bar{\lambda}/4$). The frame position with the largest modulation contrast (the best-focus frame position) should be found to minimize the focus error, and the fractional phase is measured from the best-focus position.
28. P. Hariharan, B. F. Oreb, and E. Eiju, "Digital phase-shifting interferometry: a simple error-compensating phase calculation algorithm," Appl. Opt. **26,** 2504–2506 (1987).
29. K. Creath, "Calibration of numerical aperture effects in interferometric microscope objectives," Appl. Opt. **28,** 3333–3338 (1989).
30. C. J. R. Sheppard and K. G. Larkin, "Effect of numerical aperture on interference fringe spacing," Appl. Opt. **34,** 4731–4734 (1995).
31. The coherence length of the unfiltered tungsten light source is 1.2 μm, and after the 80-nm bandpass filter at the center wavelength of 600 nm the coherence length is 2.2 μm. This coherence length (2.2 μm) is limited by the NA of the 50× objective rather than by the filter's bandwidth.[14]
32. K. Hibino, B. F. Oreb, D. I. Farrany, and K. G. Larkin, "Phase shifting for nonsinusoidal waveforms with shifting errors," J. Opt. Soc. Am. A **12,** 761–768 (1995).